Accepted Manuscript

Microstructure and compressive properties of silicon carbide reinforced geopolymer

Fei-Peng Du, Sui-Sui Xie, Fang Zhang, Chak-Yin Tang, Ling Chen, Wing-Cheung Law, Chi-Pong Tsui

PII: S1359-8368(16)31755-3

DOI: 10.1016/j.compositesb.2016.08.036

Reference: JCOMB 4484

To appear in: *Composites Part B*

Received Date: 12 March 2016

Revised Date: 15 July 2016

Accepted Date: 27 August 2016

Please cite this article as: Du F-P, Xie S-S, Zhang F, Tang C-Y, Chen L, Law W-C, Tsui C-P, Microstructure and compressive properties of silicon carbide reinforced geopolymer, *Composites Part B* (2016), doi: 10.1016/j.compositesb.2016.08.036.

Microstructure and Compressive Properties of Silicon Carbide Reinforced Geopolymer

Fei-Peng Du[1], Sui-Sui Xie[1], Fang Zhang[1], Chak-Yin Tang[2*], Ling Chen[2], Wing-Cheung Law[2], Chi-Pong Tsui[2]

1. School of Materials Science and Engineering, Wuhan Institute of Technology, Wuhan 430074, China;

2. Department of Industrial and Systems Engineering, The Hong Kong Polytechnic University, Hung Hom, Hong Kong, China.

Abstract

Geopolymers (GPs) have emerged as a promising alternative to ordinary cement due to its attractive physical and thermal properties. The typical compressive strength of geopolymers and their composites is usually limited to around 80 MPa, therefore they should be further strengthened for wider applications, such as ultrahigh strength concrete, and bone replacement. This paper presents a facile method of enhancing the compressive strength by incorporating silicon carbide particles (SiC_p) and silicon carbide whiskers (SiC_w) into the geopolymer matrix via the geopolymerization of metakaolin (MK). The effects of the reinforcement of SiC_p and SiC_w on the microstructure, thermal properties and compressive properties of the composites were investigated. The SEM images showed that both SiC_p and SiC_w were well dispersed in the geopolymer matrix. Due to the bridging effect among the SiC_w particles, SiC_w/GP composites possessed higher porosity and lower density, and thus lower thermal stability and thermal conductivity as compared with SiC_p/GP. The mechanical tests showed that the compressive strength of SiC_p/GP composites increased with the increase of SiC_p concentration. With an optimum concentration of 10 wt. % of SiC_p, the compressive strength of the composite was enhanced to 155 MPa, corresponding to a 100% increase as compared with the unfilled geopolymer.

Key words: A. Polymer matrix composites; B. Microstructures; B. Mechanical properties

*Corresponding author: Prof. CY Tang, mfcytang@polyu.edu.hk

1. Introduction

Geopolymers, as inorganic cementitious materials, have received much attraction in recent years due to their high strength, acid corrosion resistance, high temperature resistance, fire resistance, eco-friendliness, and good durability [1-3]. The formed three-dimensional networks of geopolymers exhibit the properties of organic thermoset polymers via dissolving aluminosilicate oxides to produce silicon tetrahedral ($Si(OH)_4^-$) and aluminum tetrahedral($Al(OH)_4^-$) monomers, followed by linking the two tetrahedras alternately with oxygen atoms to form polysialate chains [4-5]. Geopolymers not only show similar mechanical properties to Ordinary Portland Cement (OPC), but the CO_2 emission in the manufacture process is also significantly reduced by at least 80% [6]. Due to the simple preparation procedures, low energy consumption, low cost of raw materials and high performance, geopolymers are being considered as replacements of traditional construction materials [7, 8].

A lot of solid mineral waste, including aluminosilicate, is often used as geopolymer precursors. In particular, coal fly ash, blast furnace slag and metakaolin (MK) are considered as the major geopolymer precursors [9-15]. MK is an ideal material for conducting geopolymer research because it has relatively well-defined chemical composition, structure and properties, as compared to the large variations in chemical composition and physical properties of the coal fly ash and slag [16, 17]. In recent year, MK based geopolymers have been investigated for special applications such as the encapsulation/immobilisation of nuclear waste due to their highly stable chemical/physical properties [18-21]. From the previous reports, it was stated that the mechanical properties, such as flexural strength and compressive strength, of the MK based geopolymers could be improved by adjusting the synthesis parameters such as pH value, curing time, temperature, and the concentration and type of alkali activators [22]. Typically, the compressive strength of a MK based geopolymer can attain above 70 MPa, which is comparable to the normal concrete [23-26]. In order to extend the applications of geopolymers, such as ultrahigh-performance-concrete (over 120 MPa) [27] and human bone replacement (over 160 MPa) [28], the compressive strength of geopolymers and their composites are required to be further improved.

Besides the above-mentioned changes in the preparation process of geopolymers [22], addition of reinforcement fillers is also one of the main means to improve the compressive strength. When the filled particles have good compatibility with the

geopolymer, the improvement in the compressive strength of the resulting composites becomes significant. The compressive strength of MK based geopolymers has been enhanced by the addition of α-Al_2O_3 powder [29]. Silica fume (40 wt.%) was able to enhance the compressive strength of fly ash based-geopolymer by 51.2 % to ~73MPa [30]. The use of nano-sized fillers also improves the compressive strength of geopolymers. A geopolymer with 2.0 wt.% nano-silica achieved 67 MPa of compressive strength, which corresponded to a ~100% of enhancement [31]. Carbon-based fillers can also enhance the compressive strength. With incorporation of 1 wt.% of graphene nanoplatelets, the compressive strength of fly ash based geopolymer increased from 32 MPa to 46 MPa [32]. In addition, various types of fibers, such as polyvinyl alcohol (PVA) fibres [33, 34], steel fibers [35, 36], cotton fibres [37], and polypropylene (PP) fibres [36, 38], were used to improve the mechanical properties of geopolymers, especially the compressive properties. For instance, the compressive strength of a geopolymer reinforced with 2 vol.% of PVA fibers reached 63.7 MPa with an increase of ~17% [34]. A high compressive strength of geopolymer concrete (~175 MPa) was obtained with an addition of 13 mm steel fibers [35]. For cotton fabric reinforced geopolymer composites, an increase of 350% in compressive strength was accomplished by orienting 8.3 wt.% cotton fabric along the loading direction [37]. However, one of the major issues of reinforced geopolymer composites is the weak interfacial bonding between the filler and the geopolymer matrix, which can subsequently reduce the mechanical strength. For example, when graphite, polytetrafluoroethylene, or molybdenum disulfide was added into the geopolymers, the compressive strength of the composites decreased with increasing volume fraction of the filler due to the weak interfacial bonding [39].

SiC_p and SiC_w are the ideal inorganic fillers for reinforcing and toughening the metal matrix and ceramics due to their high mechanical performance and good compatibility with the matrix [40, 41]. In this study, MK was firstly reactivated and then SiC_p and SiC_w were utilized to reinforce the MK based geopolymers. The effect of the concentration and the dimensions of the fillers on the microstructure and compressive properties of the composites were evaluated. The results showed that the shape of the SiC filler plays an important role for improving the compressive strength of MK based geopolymers.

2. Experimental section

2.1 Materials and reagents

Superfine MK powders with an average diameter of 3.5 μm were purchased from the Aladdin Industrial Corporation. The superfine grade of the MK powders was used to improve their dissolving rate in an alkaline solution. Sodium silicate was purchased from Jiangxi Nanchang Mingrui Chemical Co., Ltd (China) with the 3.1~3.4 module of SiO_2/Na_2O. SiC_p with the average diameter of ~700 nm and SiC_w (90% purity) with an average length of ~30 μm and an average diameter of ~300 nm were purchased from Qinhuangdao Eno Material Co., Ltd (China). Other reagents were purchased from Shanghai Sinopharm Chemical Reagent Co., Ltd (China).

2.2 Preparation of geopolymers

Before preparing the reactive slurry, metakaolin (MK) powders were reactivated at 750°C for 2 hours to obtain highly reactive MK (r-MK) as the primary Si and Al sources. The mole ratio of the Si/Al in the geopolymer determines their types of molecular configuration. When the mole ratio of Si/Al is 2:1, geopolymers have high strength theoretically due to the structure of poly-sialate-siloxo (PSS type) [10, 42-44]. It has been found from other studies [2, 7, 25] that the compressive strength and other physical properties are optimal when the mole ratio of Si/Al is in the range of 1.4-2.0. Therefore, the geopolymers with three different mole ratios of Si/Al, namely 1.3, 1.5 and 1.7, were prepared. To prepare the geopolymer with the Si/Al mole ratio of 1.5, the reactive slurry was prepared as follows: 1g of sodium hydroxide (NaOH) was dissolved in deionized water (1.5 ml) to form a homogenous solution, and then 7.27 g of sodium silicate was mixed with the NaOH solution to form alkali activators and aged for 24 hours. 6.9 g of the r-MK was subsequently added to the alkali activators under grinding for 30 minutes.

The formed precursor slurry was transferred to a polytetrafluoroethylene (PTFE) mould, and kept at an ambient temperature for 24 hours. The slurry was then kept in a sealed box for curing at 40°C for 1 day, 50°C for 4 days and 60°C for another 2 days. Finally, the unsealed precursors were autoclaved at 80°C and 100°C for 2 and 4 hours, respectively, for further polymerization and hardening. After demoulding, the

geopolymers were fabricated after 28-day curing under atmospheric conditions at room temperature. The sizes of the obtained samples were tailored to 20 mm × 20 mm (diameter, Φ × height, h) for compression testing. To adjust the amount of the sodium silicate and the r-MK, the other two kinds of geopolymers with the Si/Al mole ratios of 1.3 and 1.7 were separately prepared. The compressive strength of the geopolymers with the Si/Al mole ratios of 1.3, 1.5 and 1.7 were 45 MPa, 77MPa and 68 MPa respectively. Therefore, the geopolymer with the Si/Al ratio of 1.5 was chosen for preparation of its composites.

2.3 Preparation of geopolymer composites

The preparation of geopolymer composites is similar to that of unfilled geopolymer. During the preparation process, 1wt.%, 5wt.% and 10wt.% SiC fillers were added to the slurry of alkali activators and r-MK under grinding for 30 minutes, respectively. The formed precursor slurry was transferred to another PTFE mould, and processed using the same curing process as the unfilled geopolymer.

2.3 **Characterization**

X-ray diffraction (XRD) patterns were obtained using a Bruker D8 Advance X-ray diffraction instrument (Cu Kα radiation, 0.15841 nm of wavelength) with 0.02° step width and 10°~80° scanning range. Thermogravimetric (TG) and differential scanning calorimetric (DSC) analyses were done via NETZSCH STA-409 PC thermal analyzer at a heating rate of 10 °C min^{-1} in a flowing nitrogen atmosphere. The thermal conductivity was measured with a steady-state thermal conductivity meter (TC-II, Shanghai Fudan Tianxin Co., Ltd.) [45]. Scanning electron microscopy (SEM) was conducted using a JEOL JSM-5510LV scanning electron microscope. Tests on the compressive properties were carried out via a computerized electronic universal testing machine (WDW-50, Shanghai Yu Chen Instrument Co., Ltd., China) at a loading velocity of 2 N/s.

3. Results and Discussion

3.1 Influences of constituents for preparation of geopolymers

The alkaline activator was used to dissolve the r-MK [22-24]. At the same time, alkali

cations Na^+ balanced the negative charge of Al^{3+} in IV-fold coordination and existed in the cavities of the geopolymer network with 2 mole of IV-fold coordinated Al^{3+} requiring 1 mole of Na_2O for electrical neutrality theoretically [42]. Therefore, the alkaline activator has important influence on the polymerization rate and stability of geopolymers. The size of aggregates also has effect on the polymerization process [46].

In addition, water has three functions in the geo-polymerization process: transporting ions, assisting in forming polymer chains, and regulating the flowability of the reacting precursor. As a relative high water/solids ratio decreased the compressive strength and elastic modulus of the geopolymers [1], the geopolymer composites in this work were prepared by using the Si/Al mole ratio of 1.5, SiO_2/Na_2O mole ratio of 4, H_2O/Na_2O mole ratio of 16, and 4 M of NaOH. On the other hand, it should be noted that geopolymers and their composites would crack and thus have poor mechanical properties when the reaction temperature is too high during the preparation process [24, 25].

In order to shorten the preparation period and avoid cracking, a temperature route was developed by dissolving the solid MK at room temperature for 1 day and 40°C for 1 day with polymerization at 50 °C for 4 days and 60°C for another 2 days, and subsequent hardening at 80 °C and 100°C for 2 and 4 hours, respectively. Moreover, all samples were placed into a sealed bag to slow down the evaporation rate of water and avoid cracking. Fig. 1 shows an as-prepared cylindrical geopolymer sample based on our chosen preparation process with no obvious cracks found.

If the MK has a low reactivity, the formation of the geopolymer is difficult. Therefore, the MK as-received needs further heat treatment to obtain high reactivity. Fig. 2 shows the XRD patterns of the MK, r-MK, and r-MK based geopolymers. It can be seen that MK and r-MK have similar XRD patterns. The diffused halo peaks between 18° and 25° in Fig.2(a) and (b) are attributed to the amorphous structure of MK framework. The small sharp peaks at 26°, 47° and 67° can be identified as the quartz crystal structure in the MK and r-MK samples [29]. Therefore, the amorphous structure of MK was retained after the calcinating process at 750 °C. From curve (c), the crystalline peaks for quartz are still observed as the major crystalline phase in the

samples, indicating that no reaction took place between the quartz and the alkali activator. When comparing the XRD patterns of geopolymers, MK and r-MK, there were no new peaks in the curves of geopolymer and no other crystalline phases were formed. However, it was found that the weak hump peak at ~22° disappears and a prominent amorphous hump appears between 25° and 30° from the XRD pattern of the geopolymer, implying that the aluminosilicate of r-MK resulted in the formation of a new amorphous structure in the process of geopolymer formation [47, 48].

Fig. 3 shows the SEM images of MK, r-MK and their geopolymers. Both the MK and r-MK show agglomeration or a fused flake-like structures with sizes ranging from 300 nm to 5 μm (Fig. 3 (a, b)). The SEM images show that the reactivation of MK to r-MK did not induce any changes to the typical hexagonal morphology of MK. The effect of MK and r-MK on the morphology of the geopolymer after the polymerization can be observed via SEM images. In Fig.3(c) and (d), it can be seen that there are more grains (large particles) in the cross-section of the MK based geopolymer, while there are less grains, and a more uniform and continuous thick gel phase, in the r-MK based geopolymer, suggesting that the r-MK was fully activated by the alkali activator to form a polymer gel network structure.

It can be inferred that the calcination can further remove the constituted water in the interlayer structure of MK and further make the residual six-coordinate aluminum transform to four-coordinate aluminum [49, 50]. In Fig. 4, the DSC curve shows that there are four changes of enthalpy during the temperature range from 40ºC to 1000ºC. There is a small broad endothermic peak at ~117ºC, indicating the volatilization of the adsorbed water on the surface of the MK particles [51]. Another strong endothermic peak occurs at ~389ºC, and can be related to the removal of the interlayer structural water in MK. The dehydroxylation of the residual hydroxyl in the structure of MK leads to another strong endothermic peak at ~677ºC [52], and the broad exothermic peak at ~915ºC indicates the transfer of amorphous metakaolin to mullite crystal [52]. Based on the DSC data, the TG curve can be readily interpreted. The mass loss is relatively small for the whole process from 40ºC to 1000ºC, with an only about 14 wt.%. Volatilization of the adsorbed water on the surface of the MK particles resulted in a mass loss of about 2.3 wt.% from 40 ºC to 200ºC. About 5.4 wt.% of the mass

loss was caused by the removal of the interlayer structural water of MK between 200ºC and 500ºC. ~5 wt.% of the mass loss between 500ºC to 900ºC can be mainly attributed to the dehydroxylation of MK structure, and the crystalline transform led to ~1wt.% of mass loss from 900ºC to 1000ºC. Therefore, r-MK was in a higher metastable stage after calcination and easier to activate by an alkaline activator compared to MK due to the removal of the interlayer water and further dehydroxylation of MK. The MK particles without reactivation had a low reactive activity and the alkali activator only functioned on their surface so that the residual particles contacted with each other via the bonding of the gel on their surface. Contrarily, the r-MK had a higher reactivity and could be easily modified by the alkali activator, forming new chain structures [1-3].

3.2 Microstructure of geopolymer composites

The XRD patterns of the SiC_p and SiC_w based geopolymer composites exhibit little difference as shown in Fig.5. The XRD patterns of both the SiC_p and SiC_w samples have three main crystal peaks (35.8°, 60°, and 72°), which correspond to the SiC standard card 650360. Besides the crystal peaks of SiC, there were broad hump peaks between 25°-30° in the XRD patterns of both composites, indicating the presence of amorphous geopolymer gel. The small crystal peaks at 26°, 47° and 67°, which correspond to the quartz peaks, are still observed in Fig.5, suggesting that the crystal structure of quartz was retained during the geopolymerization.

In **Table 1**, it can be seen that the apparent densities of both SiC_p/GP and SiC_w/GP were altered slightly due to the effect of the fillers. Moreover, the porosity of SiC_w/GP had a larger difference as compared with the geopolymer and SiC_p/GP. It is noted that all the geopolymer composite samples had a lower density than the geopolymer. It is due to the fact that voids were produced from the water evaporation process during the formation of the geopolymer. It is an important process since it is also a way to prepare a light-weight porous geopolymer. Moreover, the variations of density and porosity could be related to the degree of packing of the fillers in the matrix [53]. Spherical particles in the matrix easily pack into compact structures, resulting in the geopolymer composites with low porosity and high density. In contrast, fibers and whiskers readily led to formation of voids due to their high aspect ratio and strong

bridge effect among whiskers, resulting in high porosity and low density. Therefore, the porosity of SiC_w/GP increased with the increase of SiC_w content.

Fig. 6 shows the SEM images of the SiC fillers and their geopolymer composites. Most of the SiC_p is irregularly shaped with a broad distribution of size between 200 nm and 2 μm (Fig. 6a). SiC_w has a high aspect ratio (>100), length 10-50 μm and diameter 100-600 nm (Fig.6(b)). As shown in Fig. 6(c) and (d), the SiC_ps are uniformly dispersed into the geopolymer matrix and the as-prepared geopolymers are in a continuous thick gel phase, similar to the organic polymer matrix. Moreover, the particles are tightly embedded in the matrix. The grain size in 10 wt.% SiC_p/GP is larger than in 1 wt.% SiC_p/GP, which may have resulted from the aggregation of particles due to the high loading content. The microstructure of SiC_w/GP in Fig.6(e) and (f) illustrate that the SiC_w is also dispersed in the geopolymer matrix. On the one hand, the good interfacial bonding between the fillers and geopolymer originates from the good compatibility of SiC and geopolymer. SiC has good hydrophilicity such that both SiC_p and SiC_w have good compatibilities with the geopolymer matrix. On the other hand, the strong interfacial bonding could be attributed to the polymerization of geopolymer precursor that produced the tightly wrapped chain structure of the SiC_p and SiC_w. As observed from the cross-section of SiC_w/GP and SiC_p/GP, there are more voids formed in SiC_w/GP than in SiC_p/GP (identified by arrows). Moreover, a higher whisker content led to more void formation compared to a low whisker content, as shown in Fig. 6(e) and (f). The void variation with the filler content observed in the SEM images shows good agreement with the porosity data shown in Table 1, and can be attributed to the bridge effect among the whisker fillers [53].

3.3 Thermal properties

TGA curves in Fig.7 show that there are two stages for mass losses of the geopolymer and geopolymer composites. The first stage was due to the loss of physically adsorbing water between 40ºC and 300ºC. As the composites with high porosity absorb more water physically, the mass losses of SiC_p/GP composites are lower than those of SiC_w/GP composites in the first stage, which is similar to the previous report [54]. The second stage was attributed to decomposition of the chemically bonded

water and dehydroxylation of the geopolymer chains between 300ºC and 900ºC. During the whole testing temperature range, the mass losses of the unfilled geopolymer, 10wt.% SiC_p/GP, and 10wt.% SiC_w/GP are 5.8%, 6.6%, and 9.5%, respectively as in Fig.7. Therefore, the unfilled geopolymer has higher thermal stability due to full polycondensation. Although this is the case, the composite with high content (e.g. 10wt.%) of SiC_p also has good thermal stability comparable to that of the unfilled geopolymer. Moreover, the thermal stability of SiC_p/GP is better than that of SiC_w/GP because SiC_p/GP had lower porosity, and more chemically bonded water and hydroxyl groups were present in the pores and the phase interfaces of SiC_w/GP.

Figure 8 shows the thermal conductivities of the unfilled geopolymer and geopolymer composites. The thermal conductivity of the unfilled geopolymer is 0.7929 $W/m^{-1} \cdot K^{-1}$, which is similar to the previous report [55]. It can be found that the thermal conductivities of geopolymers increase with increasing content of SiC_p or SiC_w, because the SiC particles and whiskers are excellent thermal conductive fillers [56-57]. Therefore, thermal conductivity of 10 wt.% SiC_w/GP is 0.7674 $W/m^{-1} \cdot K^{-1}$, which is higher than that of 1 wt.% SiC_w/GP with by 14.5%. Moreover, the thermal conductivity of 10wt. % SiC_p/GP increases more significantly by 28.6% to 0.9474 $W/m^{-1} \cdot K^{-1}$ from 0.7369 $W/m^{-1} \cdot K^{-1}$ for the composite with only 1 wt.% SiC_p. It should be noted that thermal conductivity of the composites not only depends on the filler content but also their porosity, and has been reported to decrease with increasing porosity [58]. Hence, the thermal conductivities of 5 wt.% SiC_p/GP and 10 wt.% SiC_p/GP are better than those of unfilled geopolymer and SiC_w/GP composites because of lower porosity in the SiC_p/GP composites.

3.4 Compressive properties

The compressive strength of SiC_p and SiC_p reinforced geopolymer composites is shown in Fig.9. The compressive strength of the as-prepared geopolymer without fillers is 77 MPa, which is similar to the values in previous reports [26, 59]. The

compressive strength of 1 wt.% SiC_p/GP is 87 MPa. After the addition of 5 wt.% SiC_p, the compressive strength of the geopolymer composites increased to 115 MPa, corresponding to a 49% increase as compared to the unfilled geopolymer. When the content of SiC_p was further increased to 10 wt.%, the SiC_p/GP had a compressive strength of 155 MPa (~100% of enhancement).

For SiC_w/GP, when the filler content was low (1 wt.%), the compressive strength decreased slightly by 11.7%. Furthermore, when the SiC_w content was increased to 5 wt.%, the compressive strength decreased sharply by 51 % to 38 MPa as compared to the geopolymer. The compressive strength further decreased to 22 MPa when the SiC_w content increased to 10 wt.%. It is inferred that the deterioration of the compressive strength resulted from the bridging effect among the whiskers. When the SiC_w content was low, the bridging effect was weak and few voids were produced in the bulk of the SiC_w/GP. Thus, the compressive strength only slightly declined. However, a high content of whiskers led to a more significant bridging effect and formation of many voids after the polymerization. The low density and high porosity of the composites have a negative influence on the compressive strength, similar to the values in previous reports [60, 61].

Table 2 shows a **c**omparison for the compressive strength of the geopolymers and their composites between those reported in the open literatures and our specimens. One can see that in our work, the optimized process and concentration of GP/SiC_p, led to a significant improvement of compressive strength (~155 MPa) which is comparable to that of the steel fiber reinforced geopolymer [35]. This value is close to the level of human bone [28] and reaches the level of superhigh strength concrete [27].

4. Conclusions

In this work, SiC_p/GP and SiC_w/GP samples were successfully prepared. r-MK was readily activated by alkali activator to form an excellent geopolymer cementitious material. The hydrophilicity of SiC and the binding of the inorganic polymer network resulted in a strong interfacial bonding between the SiC filler and geopolymer. However, the difference in packing mode for particles and whiskers in the geopolymer matrix resulted in a difference of porosity and density of the geopolymer

composites. The bridging effect among the whiskers led to low density and high porosity of SiC_w/GP, impairing their compressive properties and weakening their thermal stability and thermal conductivity as compared with the SiC_p/GP and the unfilled geopolymer. Therefore, the porosity resulted from the addition of filler must be carefully optimized in strengthening the compressive properties of geopolymers. The enhanced compressive strength (>150 MPa) will enable further exploration of the potential uses of this material for making superhigh strength concrete and bone replacement devices.

Acknowledgements

We would like to acknowledge funding support from the Natural National Science Foundation of China (51373126), the Research Committee of The Hong Kong Polytechnic University (Project Code: G-YL93), and the Science Research Council of the Wuhan Institute of Technology (k201463).

References

[1]Nematollahi B, Sanjayan J, Shaikh FUA. Matrix design of strain hardening fiber reinforced engineered geopolymer composite. Compos Part B-Eng 2016; 89: 253-65.

[2] Menna C, Asprone D, Ferone C, Colangelo F, Balsamo A, Prota A, Cioffi R, Manfredi G. Use of geopolymers for composite external reinforcement of RC members. Compos Part B-Eng 2013; 45, 1667-76.

[3]Masi G, Rickard WDA, Bignozzi MC, van Riessen A. The effect of organic and inorganic fibres on the mechanical and thermal properties of aluminate activated geopolymers. Compos Part B-Eng, 2015; 76: 218-28.

[4] Hajimohammadi A, Provis JL, van Deventer JSJ. Effect of alumina release rate on the mechanism of geopolymer gel formation. Chem Mater 2010; 22: 5199-208.

[5]Balcikanli M, Ozbay E. Optimum design of alkali activated slag concretes for the low oxygen/chloride ion permeability and thermal conductivity. Compos Part B-Eng 2016; 91: 243-56

[6] Fan X, Zhang M. Experimental study on flexural behaviour of inorganic polymer concrete beams reinforced with basalt rebar. Compos Part B-Eng 2016; 93: 174-83.

[7] Bernal SA, Bejarano J, Cristhian G, de Gutiérrez RM, Delvasto S, Rodríguez ED. Performance of refractory aluminosilicate particle/fiber-reinforced geopolymer

composites. Compos Part B-Eng 2012; 43: 1919-28.

[8]Allison PG, Weiss jr. CA, Moser RD, Diaz AJ, Rivera OG, Holton SS. Nanoindentation and SEM/EDX characterization of the geopolymer-to-steel interfacial transition zone for a reactive porcelain enamel coating. Compos Part B-Eng 2015; 78: 131–7.

[9] Görhan G, Kürklü G. The influence of the NaOH solution on the properties of the fly ash-based geopolymer mortar cured at different temperatures. Compos Part B-Eng 2014; 58: 371-7.

[10] Zivica V, Palou MT, Bágeľ TIĽ. High strength metahalloysite based geopolymer. Compos Part B-Eng 2014; 57: 155-65.

[11] Bohlooli H, Nazari A, Khalaj G, Kaykha MM, Riahi S. Experimental investigations and fuzzy logic modeling of compressive strength of geopolymers with seeded fly ash and rice husk bark ash. Compos Part B-Eng 2012; 43, 1293-301.

[12]Ma Y, Hu J, Ye G. The effect of activating solution on the mechanical strength, reaction rate, mineralogy, and microstructure of alkali-activated fly ash. J Mater Sci 2012; 47: 4568-78.

[13]Gunasekara C, Law DW, Setunge S, Sanjayan JG. Zeta potential, gel formation and compressive strength of low calcium fly ash geopolymer. Constr Build Mater 2015; 95: 592-9.

[14] Alomayri T, Shaikh FUA, Low IM. Synthesis and mechanical properties of cotton fabric reinforced geopolymer composites. Compos Part B-Eng 2014; 60: 36-42.

[15] Alomayri T, Shaikh FUA, Low IM. Characterisation of cotton fibre-reinforced geopolymer composites. Compos Part B-Eng 2013; 50: 1-6.

[16]Fernández-Jiménez A, Zibouche F, Boudissa N, García-Lodeiro I, Abadlia MT, Palomo A. “Metakaolin-Slag-Clinker Blends.” The role of Na^+ or K^+ as alkaline activators of theses ternary blends. J Am Ceram Soc 2013; 96: 1991-98.

[17]Balczár I, Korim T, Dobrádi A. Correlation of strength to apparent porosity of geopolymers-Understanding through variations of setting time. Constr Build Mater 2015; 93: 983-8.

[18]Bell JL, Driemeyer PE, Kriven WM. Formation of ceramics from metakaolin based geopolymers. Part II: K-based geopolymer. J Am Ceram Soc 2009; 92: 607-15.

[19]Bell JL, Driemeyer PE, Kriven WM. Formation of ceramics from metakaolin

based geopolymers: Part I: Cs-based geopolymer. J Am Ceram Soc 2009; 92: 1-8.

[20]Blackford MG, Hanna JV, Pike KJ, Vance ER, Perera DS. Transmission electron microscopy and nuclear magnetic resonance studies of geopolymers for radioactive waste immobilization. J Am Ceram Soc 2007; 90: 1193-9.

[21]Kuenzel C, Vandeperre L, Cheeseman CR, Boccaccini AR. Geopolymers for the encapsulation of solid nuclear waste. Decommissioning, Immobilisation and Management of Nuclear Waste Disposal, 2010 Manchester, UK.

[22]Kuenzel C, Neville TP, Donatello S, Vandeperre L, Boccaccini AR, Cheeseman CR. Influence of metakaolin characteristics on the mechanical properties of geopolymers. Appl Clay Sci 2013; 83-84: 308-14.

[23]Gharzouni A, Joussein E, Samet B, Baklouti S, Pronier S, Sobrados I, Sanz J, Rossignol S. The effect of an activation solution with siliceous species on the chemical reactivity and mechanical properties of geopolymers. J Sol-Gel Sci Techn 2015; 73:250-9.

[24]Cheng H, Lin KL, Cui R, Hwang CL, Chang YM, Cheng TW. The effects of SiO_2/Na_2O molar ratio on the characteristics of alkali-activated waste catalyst-metakaolin based geopolymers. Constr Build Mater 2015; 95: 710-20.

[25]Ozer I, Soyer-Uzun S. Relations between the structural characteristics and compressive strength in metakaolin based geopolymers with different molar Si/Al ratios. Ceram Int 2015; 41: 10192-8.

[26]Mo B, Zhu H, Cui X, He Y, Gong S. Effect of curing temperature on geopolymerization of metakaolin-based geopolymers. Appl Clay Sci 2014; 99: 144-8.

[27] Su Y, Li J, Wu C, Wu P, Li Z. Influences of nano-particles on dynamic strength of ultra-high performance concrete. Compos Part B-Eng 2016; 91: 595-609.

[28]Liebschner MAK. Biomechanical considerations of animal models used in tissue engineering of bone. Biomaterials 2004; 25: 1697-714.

[29]Sarkara M, Dana K, Das S. Microstructural and phase evolution in metakaolin geopolymers with different activators and added aluminosilicate fillers. J Mol Struct 2015; 1098: 110-8.

[30]Okoye FN, Durgaprasad J, Singh NB. Effect of silica fume on the mechanical properties of fly ash based-geopolymer concrete. Ceram Int 2016; 42: 3000-6.

[31]Deb PS, Sarker PK, Barbhuiya S. Effects of nano-silica on the strength development of geopolymer cured at room temperature. Constr Build Mater 2015;

101: 675-83.

[32]Ranjbar N, Mehrali M, Mehrali M, Alengaram UJ, Jumaat MZ. Graphene nanoplatelet-fly ash based geopolymer composites. Cement Concrete Res 2015; 76: 222-31.

[33]Ohno M, Li VC. A feasibility study of strain hardening fiber reinforced fly ash-based geopolymer composites. Constr Build Mater 2014; 57: 163-8.

[34]Nematollahi B, Sanjayan J, Shaikh FUA. Comparative deflection hardening behavior of short fiber reinforced geopolymer composites. Constr Build Mater 2014; 70: 54-64.

[35]Ambily PS, Ravisankar K, Umarani C, Dattatreya JK, Iyer NR. Development of ultra-high-performance geopolymer concrete. Mag Concrete Res 2014; 66: 82-9.

[36]Ranjbar N, Talebian S, Mehrali M, Kuenzel C, Metselaar HSC, Jumaat MZ. Mechanisms of interfacial bond in steel and polypropylene fiber reinforced geopolymer composites. Compos Sci Technol 2016; 122: 73-81.

[37]Alomayri T, Shaikh FUA, Low IM. Effect of fabric orientation on mechanical properties of cotton fabric reinforced geopolymer composites. Mater Design 2014; 57: 360-5.

[38]Reed M, Lokuge W, Karunasena W. Fibre-reinforced geopolymer concrete with ambient curing for in situ applications. J Mater Sci 2014; 49: 4297-304.

[39]Wang H, Li H, Yan F. Synthesis and tribological behavior of metakaolinite-based geopolymer composites. Mater Lett 2005; 59: 3976-81.

[40]Lio S, Watanabe M, Matsubara M, and Matsuo Y. Mechanical properties of Alumina/silicon carbide whisker composites. J Am Ceram Soc 1989; 72: 1880-4.

[41]Logsdon WA, Liaw PK.Tensile, fracture toughness and fatigue crack growth rate properties of silicon carbide whisker and particulate reinforced aluminum metal matrix composites. Eng Fract Mech 1986; 24: 737-51.

[42] Zhang Y, Sun W, Li Z. Composition design and microstructural characterization of calcined kaolin-based geopolymer cement. Appl Clay Sci 2010; 47: 271-5.

[43] Davidovits J. Geopolymers and geopolymer new materials. J Therm Anal 1989; 35: 429-44.

[44] Görhan G, Aslaner R, Şinik O. The effect of curing on the properties of metakaolin and fly ash-based geopolymer paste. Compos Part B-Eng 2016; 97:

329-35.

[45] Du FP, Yang W, Zhang F, Tang CY, Liu SP, Yin L, Law WC. Enhancing the heat transfer efficiency in graphene-epoxy nanocomposites using a magnesium oxide-graphene hybrid structure. ACS Appl Mater Interfaces 2015; 7: 14397-403.

[46] Ozbakkaloglu T, Xie T. Geopolymer concrete-filled FRP tubes: Behavior of circular and square columns under axial compression. Compos Part B-Eng 2016; 96: 215-30.

[47]Lizcano M, Gonzalez A, Basu S, Lozano K, Radovic M. Effects of water content and chemical composition on structural properties of alkaline activated metakaolin-based geopolymers. J Am Ceram Soc 2012; 95: 2169-77.

[48]Luukkonen T, Sarkkinen M, Kemppainen K, Rämö J, Lassi U. Metakaolin geopolymer characterization and application for ammonium removal from model solutions and landfill leachate. Appl Clay Sci 2016; 119: 266-276.

[49]Wang H, C Li, Peng Z, Zhang S. Characterization and thermal behavior of kaolin. J Therm Anal Calorim 2011; 105: 157-60.

[50]Shvarzman A, Kovler K, Grader GS, Shter GE. The effect of dehydroxylation/ amorphization degree on pozzolanic activity of kaolinite. Cement Concrete Res 2003; 33: 405-16.

[51] Douiri H, Louati S, Baklouti S, Arous M, Fakhfakh Z. Enhanced dielectric performance of metakaolin–H_3PO_4 geopolymers. Mater Lett 2016; 164: 299-302.

[52] Bich Ch, Ambroise J, Péra J. Influence of degree of dehydroxylation on the pozzolanic activity of metakaolin. Appl Clay Sci 2009; 44(3-4): 194-200.

[53]Yih P, Chung DDL. Silicon carbide whisker copper-matrix composites fabricated by hot pressing copper coated whiskers. J Mater Sci 1996; 31: 399-406.

[54]He P, Jia D, Wang M, Zhou Y. Effect of cesium substitution on the thermal evolution and ceramics formation of potassium-based geopolymer. Ceram Int 2010; 36: 2395-400.

[55]Duxson P, Lukey GC, van Deventer JSJ. Thermal conductivity of metakaolin geopolymers used as a first approximation for determining gel interconnectivity. Ind Eng Chem Res 2006; 45: 7781-8.

[56] Crocombette JP, Gelebart L. Multiscale modeling of the thermal conductivity of polycrystalline silicon carbide. J Appl Phys 2009; 106: 083520.

[57]Li Y, Huang X, Hu Z, Jiang P, Li S, Tanaka T. Large dielectric constant and high

thermal conductivity in poly(vinylidene fluoride)/barium titanate/silicon carbide three-phase nanocomposites. ACS Appl Mater Interfaces 2011; 3: 4396-403.

[58]Kamseu E, Ceron B, Tobias H, Leonelli E, Bignozzi MC, Muscio A, Libbra A. Insulating behavior of metakaolin-based geopolymer materials assess with heat flux meter and laser flash techniques. J Therm Anal Calorim 2012; 108: 1189-99.

[59]Nazari A, Maghsoudpour A, Sanjayan JG. Boroaluminosilicate geopolymers: role of NaOH concentration and curing temperature. RSC Adv 2015; 5: 11973–9.

[60]Nevarez-Rascon A, Aguilar-Elguezabal A, Orrantia E, Bocanegra-Bernal MH. Compressive strength, hardness and fracture toughness of Al_2O_3 whiskers reinforced ZTA and ATZ nanocomposites: Weibull analysis. Int J Refract Met H 2011; 29: 333-40.

[61]Chen X, Wu S, Zhou J. Influence of porosity on compressive and tensile strength of cement mortar. Constr Build Mater 2013; 40: 869-74.

List of Tables

Table 1 The apparent density and porosity of SiC reinforced geopolymer

Table 2 Compressive strength of geopolymer composites

List of Figures

Figure 1 The photograph of geopolymer specimen

Figure 2 The XRD patterns of (a) MK, (b) r-MK, and (c) r-MK based geopolymer

Figure 3 SEM images of (a) MK, (b) r-MK, (c) MK based geopolymer and (d) r-MK based geopolymer

Figure 4 Thermal analysis of MK from 40 ºC to 1000 ºC with the rate 10 ºC/min

Figure 5 The XRD patterns of (a) SiC_p and (b) SiC_w based geopolymer composites with 10 wt. % filler content

Figure 6 SEM images of (a) SiC_p, (b) SiC_w, and (c) geopolymer composites with 1wt.% SiC_p, (d) 10 wt.% SiC_p, (e) 1 wt.% SiC_w, and (f) 10 wt.% SiC_w

Figure 7 TGA curves of geopolymer composites with different content of SiC_p and SiC_w

Figure 8 Thermal conductivity of geopolymer composites with different content of SiC_p and SiC_w

Figure 9 The compressive strength of geopolymer composites with different content of SiC_p and SiC_w.

Table 1 The apparent density and porosity of SiC reinforced geopolymer

Samples	geopolymer	SiC_p/GP			SiC_w/GP		
Filler content (wt.%)	0	1	5	10	1	5	10
Apparent density (g/cm^3)	2.40	2.23	2.36	2.25	2.07	2.15	2.16
Porosity (%)	2.90	3.00	2.50	3.14	4.14	5.48	7.30

Table 2 Compressive strength of geopolymer composites

Geopolymer material	Filler type	Filler loading	Maximum compressive strength (MPa)	Enhancement of compressive strength compared to that of the neat geopolymer (%)	Ref.
GP/Al_2O_3	Al_2O_3 powder	50 wt.%	~34	25	29
GP/SiO_2	silica fume	40 wt.%	~73	51.2	30
GP/nano-SiO_2	nano-silica particle	2.0 wt.%	~67	~100	31
GP/graphene nanoplatelet	graphene nanoplatelet	1 wt.%	46	44	32
GP/PVA fibre	PVA fibre	2 vol.%	63.7	17	34
GP/cotton fabric	cotton fabric (load vertical to fabric layers)	8.3 wt.%	90	350	37
GP/ steel fibre	steel fibres	3 wt.%	175	44	35
GP/SiC	SiC particle	10 wt.%	155	~100	This work
		5 wt.%	115	49	

Figure 1. The photograph of geopolymer specimen

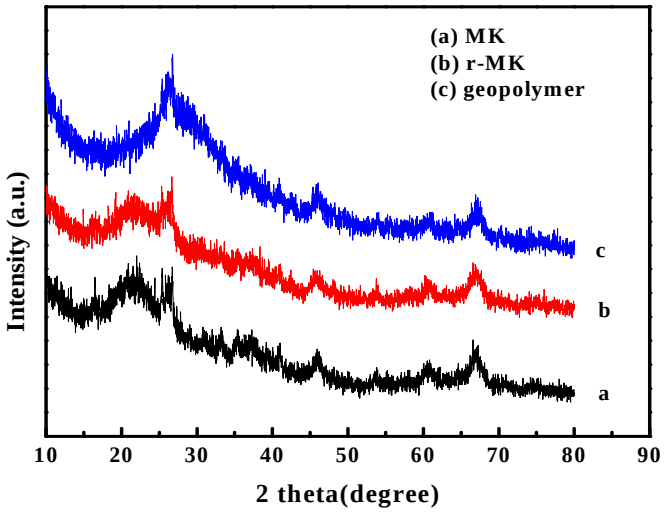

Figure 2. The XRD patterns of (a) MK, (b) r-MK, and (c) r-MK based geopolymer

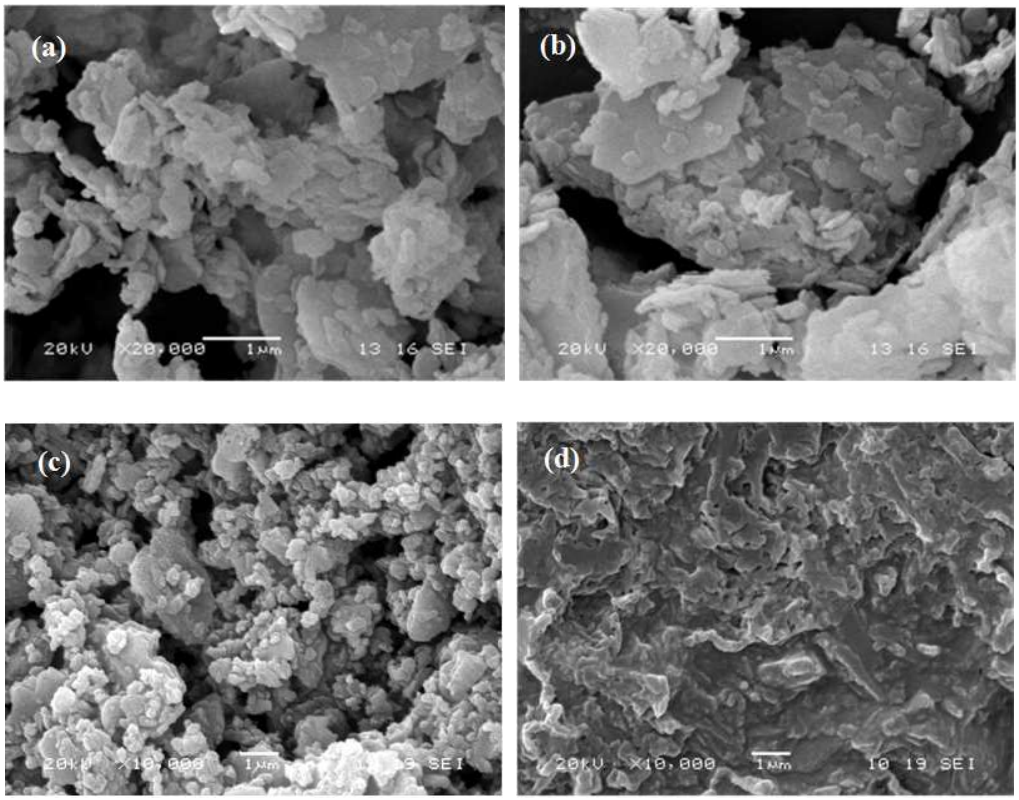

Figure 3. SEM images of (a) MK, (b) r-MK, (c) MK based geopolymer and (d) r-MK based geopolymer

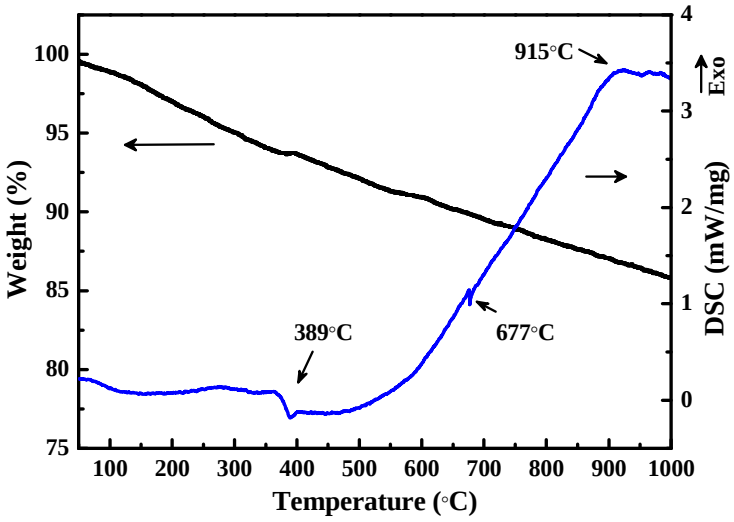

Figure 4. Thermal analysis of MK from 40 ºC to 1000 ºC with the rate 10 ºC/min

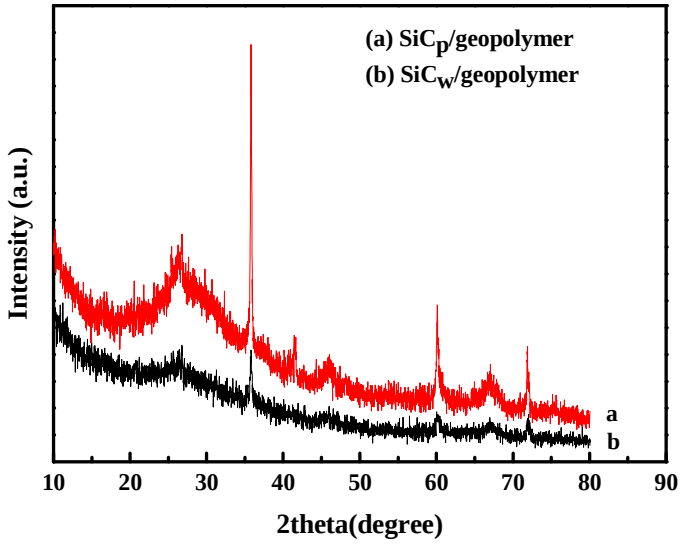

Figure 5. The XRD patterns of (a) SiC_p and (b) SiC_w based geopolymer composites with 10 wt. % filler content

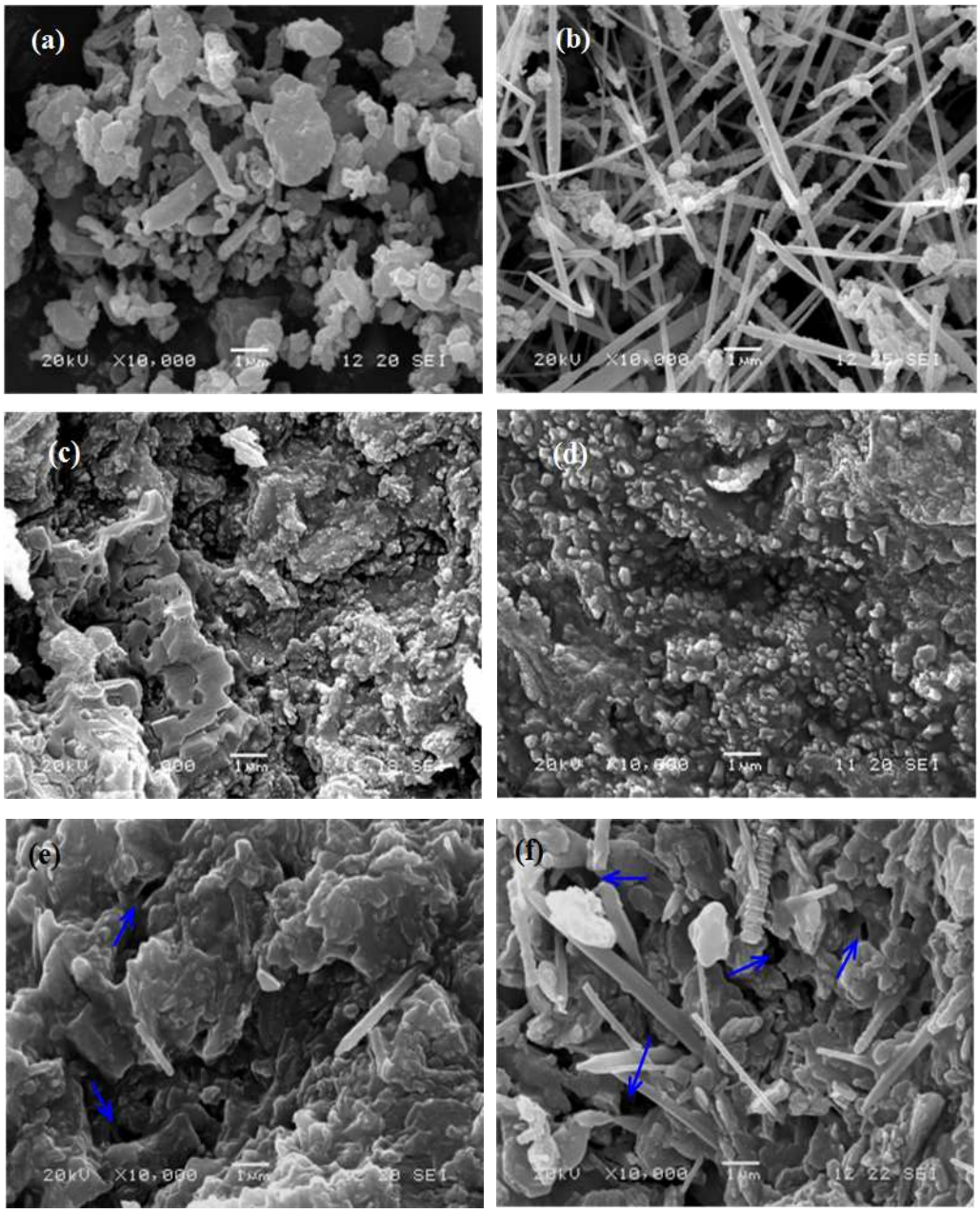

Figure 6. SEM images of (a) SiC_p, (b) SiC_w, and (c) geopolymer composites with 1wt.% SiC_p, (d) 10 wt.% SiC_p, (e) 1 wt.% SiC_w, and (f) 10 wt.% SiC_w

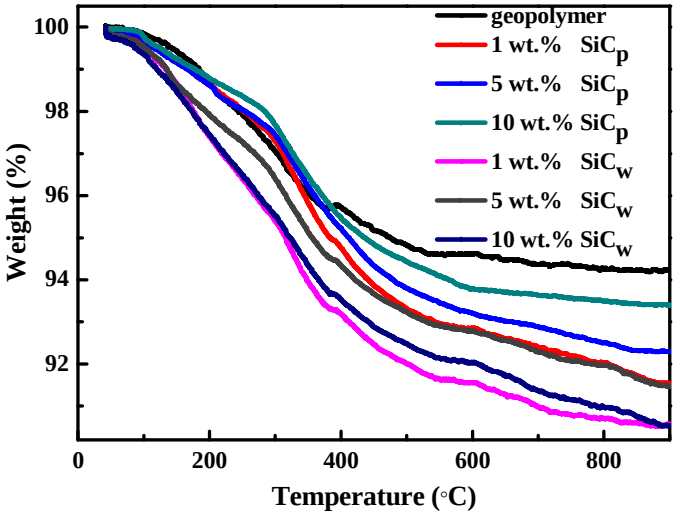

Figure 7. TGA curves of geopolymer composites with different content of SiC_p and SiC_w

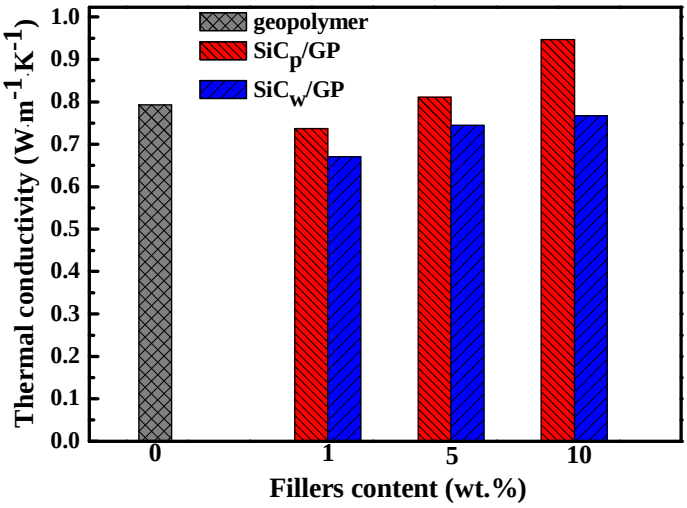

Figure 8. Thermal conductivities of geopolymer composites with different content of SiC_p and SiC_w

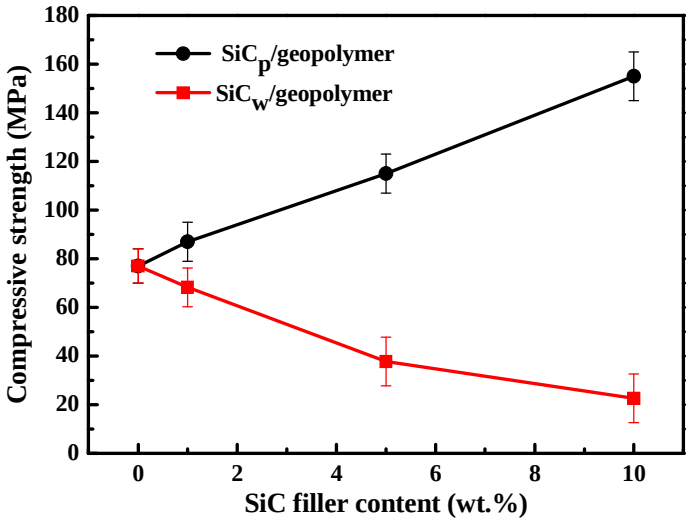

Figure 9. The compressive strength of geopolymer composites with different content of SiC_p and SiC_w.